Polymer Nanopillar–Gold Arrays as Surface-Enhanced Raman Spectroscopy Substrate for the Simultaneous Detection of Multiple Genes

Silvia Picciolini,[†,‡,∥] Dora Mehn,[†,∥] Carlo Morasso,[*,†] Renzo Vanna,[†] Marzia Bedoni,[†] Paola Pellacani,[‡] Gerardo Marchesini,[‡] Andrea Valsesia,[‡] Davide Prosperi,[§] Cristina Tresoldi,[⊥] Fabio Ciceri,[⊥] and Furio Gramatica[†]

[†]Fondazione Don Carlo Gnocchi ONLUS, Piazzale Morandi 6, 20121 Milan, Italy, [‡]Plasmore S.r.l., Via Deledda 4, 21020 Ranco, Italy, [§]NanoBioLab, Dipartimento di Biotecnologie e Bioscienze, Università degli Studi di Milano Bicocca, Piazza della Scienza 2, 20126 Milan, Italy, and [⊥]IRCCS, Ospedale San Raffaele, Via Olgettina 60, 20132 Milan, Italy. [∥]These authors contributed equally to the work.

ABSTRACT In our study, 2D nanopillar arrays with plasmonic crystal properties are optimized for surface-enhanced Raman spectroscopy (SERS) application and tested in a biochemical assay for the simultaneous detection of multiple genetic leukemia biomarkers. The special fabrication process combining soft lithography and plasma deposition techniques allows tailoring of the structural and chemical parameters of the crystal surfaces. In this way, it has been possible to tune the plasmonic resonance spectral position close to the excitation wavelength of the monochromatic laser light source in order to maximize the enhancing properties of the substrate. Samples are characterized by scanning electron microscopy and reflectance measurements and tested for SERS activity using malachite green. Besides, as the developed substrate had been prepared on a simple glass slide, SERS detection from the support side is also demonstrated. The optimized substrate is functionalized with thiol-modified capture oligonucleotides, and concentration-dependent signal of the target nucleotide is detected in a sandwich assay with labeled gold nanoparticles. Gold nanoparticles functionalized with different DNA and various Raman reporters are applied in a microarray-based assay recognizing a disease biomarker (Wilms tumor gene) and housekeeping gene expressions in the same time on spatially separated microspots. The multiplexing performance of the SERS-based bioassay is illustrated by distinguishing Raman dyes based on their complex spectral fingerprints.

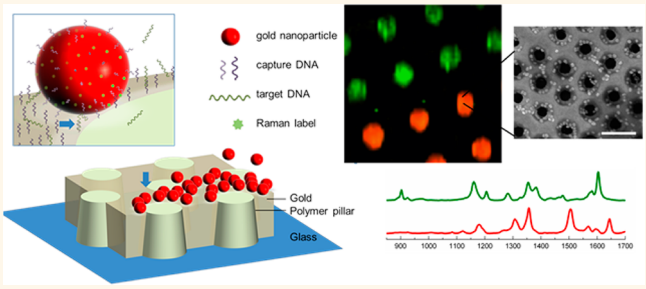

KEYWORDS: SERS · multiplex · leukemia · plasmonic · nanopillar · DNA microarray

Surface-enhanced Raman spectroscopy (SERS)-based detection of genetic biomarkers is described to provide not only high sensitivity and specificity[1] but also a better multiplexing capacity compared to the conventional clinical analytical methods.[2] These properties predestine the SERS technology to yield innovative biotechnological applications in various fields of clinical diagnostics including cancer diagnosis and monitoring.[3−5] The other peculiar feature of SERS, its extraordinary multiplexing capability arising from the Raman spectral fingerprints composed of narrow peaks, enables the simultaneous monitoring of numerous genetic markers. Multiplexing not only improves the amount of information provided by the test probing numerous disease markers at the same time but also allows the simultaneous measurement of internal controls (housekeeping genes) and by comparison of intensities also the quantification of expression levels.

A well-known example of an application where the sensitive and multiplexed biomarker detection is needed in the cancer monitoring field is the assessment of the status of leukemia patients during/after chemotherapeutical treatment. Acute myeloid leukemia (AML) is the most common leukemia in adults,[6] with about 36 000 newly diagnosed cases registered yearly in

* Address correspondence to cmorasso@dongnocchi.it.

Received for review July 15, 2014 and accepted October 3, 2014.

Published online October 03, 2014
10.1021/nn503873d

Europe and the U.S.[7] and about 10 370 deaths from AML estimated for 2013.[8] Minimal residual disease (MRD) in leukemia refers to a situation when, after the chemotherapeutic treatment, the patient seems to reach a complete remission according to conventional, morphology-based evaluations; however, residual cancer cells are still able to proliferate and to cause relapse. In addition to this, chemotherapeutical treatments might generate new mutations and lead to the artificial selection of drug-resistant cells. In fact, the induction therapy by cytarabine and daunorubicine often used in the first stage treatment of AML patients was shown to induce overexpression of multi-drug-resistant proteins such as P-gp and MRP1,[9] an important member of the ABC efflux transporter family.[10,11] Increased cure rates could be reached especially in elderly patients[12] by performing a continuous follow-up of the chemotherapeutic response that analyzes the actual level of minimal residual disease markers during and after the treatment.[13,14] Exploiting the multiplexing capacity of SERS and microarray-based gene detection, multidrug resistance, and minimal residual disease markers could be monitored simultaneously in a single assay. The most studied methods for MRD detection use molecular biological techniques and are based on real-time quantitative polymerase chain reaction (RT-PCR) or on flow cytometry. Flow cytometry is able to perform multiplexing (within the limits of fluorescent channels available in the instrument), but the method is generally less sensitive then RT-PCR. The latter can reach high sensitivity in the detection of genetic markers, but the multiplexing capacity of the method is strongly limited by the spectral overlap between fluorescent reporters.[15]

One of the most studied MRD biomarkers is the expression level of the WT1 gene mRNA transcript. WT1 expression is at present evaluated in relation to the expression of the housekeeping gene ABL and is strongly dependent on the quantity of cells analyzed to achieve appropriate levels of sensitivity. The minimum cutoff level for AML patients (between 50 and 250 WT1 copies/10^4 ABL copies) is closely associated with the type of disease and the nature of the biological samples.[16−21] In addition, for several AML subtypes, the measurement of WT1 expression must be complemented, according to clinical good practices, by monitoring other MRD markers.

Detection of the extremely low WT1 levels in blood is still technically challenging, and there is an open niche for novel analytical solutions in the sensitive, fast, and parallel quantification of more MRD and drug-resistant biomarkers, including WT1 and P-gp mRNA plasma levels.[11,14]

The efficient surface enhancement of the analyte's Raman signal requires a noble metal surface, usually nanoparticles (NPs) in suspension or nanostructured solid substrates.[22,23] Both systems have their advantages: nanoparticle suspensions are expected to provide a more homogeneous signal, while solid surfaces are easy to functionalize and use in a heterogeneous reaction system. Besides the advantage of high stability and facile phase separation, solid substrates can be patterned with capture molecules, offering the possibility of multiplexing based on the position inside the microarray. Solid SERS substrates usually profit from the so-called "*hot spot*" effect, that is, the extraordinary enhancement of the Raman signal between closely situated nanosized elements. This effect can be generated on simple irregular rough metal surfaces, but noble metal NPs deposited on various support materials,[24,25] patterns generated by electron- or ion-beam lithography, gold layer deposited on previously micropatterned surfaces,[26] or silver deposited on silicon nanowires[27] are also used as SERS substrates. Ordered 2D arrays of dielectric nanocavities or nanopillars embedded in a noble metal matrix are particularly interesting from the sensing point of view. Incoming light with proper wavelength and polarization status can be coupled with both delocalized and localized plasmonic modes supported by these structures.[28] The optical properties of these structures are strongly geometry-dependent, which allows tuning of the plasmonic resonance spectral position and regulation of transparency by changing the thickness of the metal layer, varying the shape, diameter, and distance of the nanoholes.[29] A combination of colloidal lithographic and plasma deposition methods was developed and optimized earlier to generate nanopillar arrays for surface plasmon resonance (SPR) applications.[28,30] The ordered polymeric nanopillars embedded in the continuous noble metal film behave as dielectric discontinuities, similarly to the dielectric nanocavities of a nanohole array filled with proteins, water, or a solution.

Here we present the optimization of 2D arrays of nanopillars embedded in a noble metal matrix for SERS application and their use for the development of a SERS-based DNA microarray for the detection of several genetic biomarkers obtained by combining the enhancer properties of the substrate and of functionalized gold nanoparticles (Figure 1). We demonstrate the multiplexing capacity of this system contemporarily detecting minimal residual disease markers, multidrug resistance, and housekeeping (control) genes.

RESULTS AND DISCUSSION

Morphological Analysis. Scanning electron microscopic analysis of the 2D microarrays shows hexagonally arranged polymer beads on the surface before lift-off (Figure 2D) and "hole"-like (less electron-repelling), hexagonally arranged polymer islands in the gold film after the lift-off procedure (Figure 2A−C). As it is visible in the images, the final surface is not a single crystal. Errors introduced in the self-assembled layer during

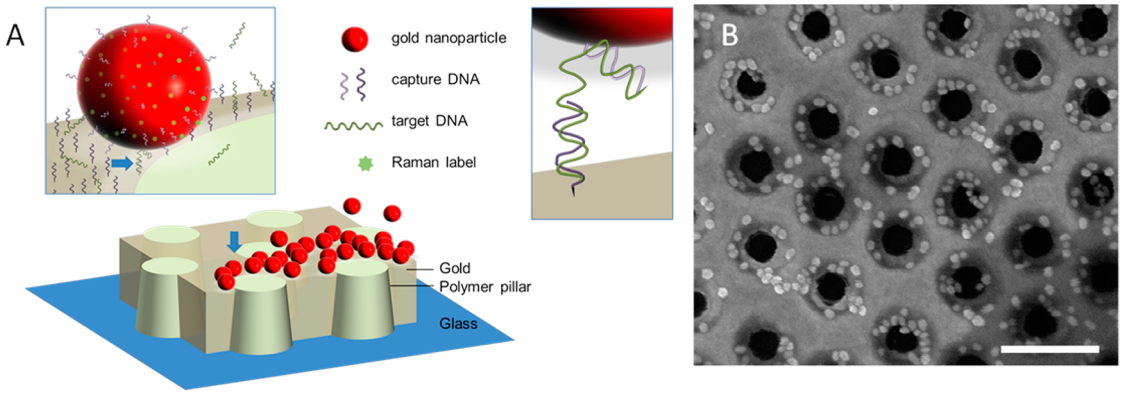

Figure 1. (A) Schematic illustration of the DNA recognition SERS assay based on the use of functionalized nanoparticle immobilization on the chip surface. Insets: (left) annealing of nonlabeled target DNA with the complementary capture sequences on the chip surface and on the nanoparticles results in particle immobilization on the surface. Raman label molecules on the nanoparticles are positioned in hot spots (bright area) generated between the particles and the localized surface plasmon; annealing of complementary sequences immobilizes nanoparticles on the gold surface. (B) SEM image of the substrate after the annealing between the sequences conjugated on the surface and on the nanoparticles. Gold nanoparticles appear as brighter spots and are mainly located around the polymeric pillars. Scale bar corresponds to 500 nm.

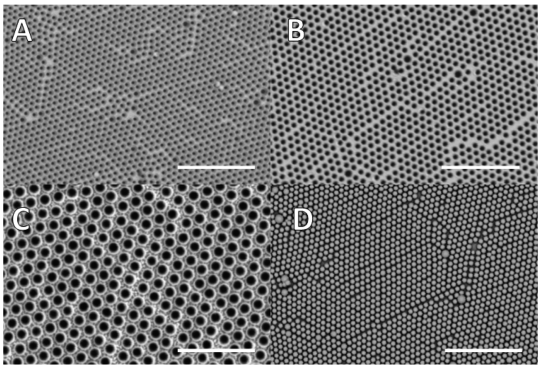

Figure 2. Scanning electron micrographs of the 2D crystal surface prepared with (A) 400 nm, (B) 500 nm, (C) 1000 nm PS beads after etching, gold deposition, and lift-off, and (D) 400 nm beads after etching, gold deposition, and before lift-off. Scale bars correspond to 5 μm in each image.

the Langmuir–Blodgett deposition of the polystyrene (PS) beads (for example, because of beads with nonregular size, Figure 2A) generate a multicrystalline surface structure. However, the size of these crystal domains (reaching thousands of microns) is large enough to provide homogeneous SERS enhancement as discussed in detail later.

The diameter of the resulting round-shaped "holes" is similar to the distance between their closest points and approximately one-half of the pitch. Thus, on a chip with 400 nm pitch, the diameter of the holes is about 200 nm and about 77% of the surface is gold-coated.

Transparent Support Features and Optimization of the Gold Thickness. Modeling of the optical behavior of perforated metal films is mostly available for noble metal nanohole arrays with a square lattice.[29] However, numerical calculations on the transmission spectrum of these types of materials suggest that the main parameters affecting the plasmonic properties are the geometrical features (pitch and hole diameter), film thickness, and composition. In samples prepared by colloidal lithography, the pitch and hole diameter are not independent because the size of the beads has an effect on both features at a given metal thickness. In our experiments, the optimal pitch of the nanopillar array was found to be wavelength-dependent at fixed (150 nm) gold thickness. In the case of 532 and 633 nm excitation wavelength, the smallest applied pitch, 400 nm, provided the most intense Raman signal with an enhancement factor up to 10^4, while the 785 nm laser gave the best results with the 1000 nm pitch sample (Figure 3A). Reflectance measurements in air (Figure 3B) indicated that the 400 nm pitch samples show a well-defined reflectance minimum at around 660 nm, and 500 nm pitch samples have one deep and a less strong minimum at around 878 and 557 nm, respectively. The 1000 nm pitch samples have a broadened spectral curve with three similar local reflectance minima at 590, 700, and 790 nm. It is notable that the most intense Raman signals are collected when the reflectance minimum of the substrate lies between the wavelength of the incoming laser light and the wavelength of the analyte's fingerprint region. (The 1000–1700 cm^{-1} range in the Raman spectrum of malachite green corresponds to wavelengths between 675 and 710 nm using a 633 nm laser, Figure 3B.)

Our results are in good agreement with the findings of Sharma *et al.*,[31] who investigated the correlation between the local surface plasmon resonance position of broad plasmon resonance silver INRA substrates and the electromagnetic field enhancement detected in SERS for these materials. They found that the electromagnetic field enhancement contribution is optimal on this type of substrate when the localized surface plasmon resonance position is situated between the excitation wavelength and the Raman-scattered

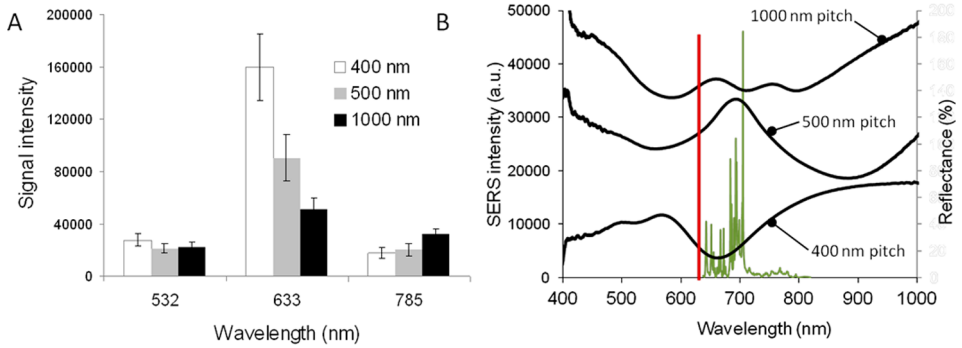

Figure 3. (A) Malachite green SERS signal intensity (peak area at 1174 1/cm, dried spots) on the chip surface at 400, 500, and 100 nm pitch (blocks in this order from left to right), at 150 nm gold thickness using 532, 633, and 785 nm excitation laser light. (B) Plasmonic band of the chips with various pitch (solid bold curves, shifted for better visibility, 1000, 500, 400 nm from top down), fingerprint region of the SERS spectrum of malachite green at 633 nm excitation on chip with 400 nm pitch (narrow spectrum lines), and position of the 633 nm excitation wavelength (vertical bold line), all in nanometer scale.

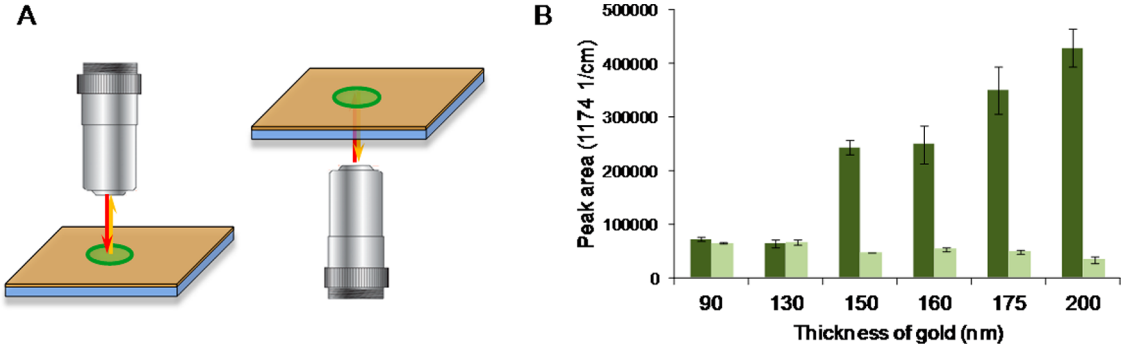

Figure 4. (A) Excitation (red arrow) and detection of scattered light (yellow arrow) from the "air side" (left) and from the "support side" (right) on the nanopillar array. (B) Malachite green SERS signal intensity (peak area at 1174 1/cm, dried spots) on the chip surface measured from the air (dark bars) and from the support side (light bars) for 400 nm pitch samples at 633 nm excitation wavelength.

photon wavelength, allowing interaction with both incident and scattered fields, as in the case of our 400 nm samples used with a 633 nm excitation.

The plasmonic resonance between the 400 nm pitch samples and the 633 nm laser light resulted in the best observed intensity values for more tested molecules including malachite green, having a spectral fingerprint region in the 1000−1700 cm^{-1} Raman shift range (Figure 3B). Thus, 400 nm pitch samples with various gold thicknesses were used to test the effect of the thickness of the structure on Raman signal enhancement. Gradual improvement of the signal was registered from the air side (Figure 4B, dark bars) with increasing gold (and polymer) thickness above 130 nm at 633 excitation wavelength. While structures with 400 nm pitch and 200 nm gold thickness functioned well, scanning electron microscopy (SEM) images showed incomplete bead removal in the case of these samples, resulting from trapping the etched particles in the relatively thick metal coating. This effect limits the geometrical tunability of the 2D nanopillar arrays generated by colloidal lithography as the resulting polymer pillars are covered by a gold-coated polymer bead sitting on top of the pillars.

Nanohole arrays are known to show extraordinary transmission due to the localized surface plasmonic resonance given by the presence of the dielectric nanocavities in the noble metal film. This allows "communication" with the other side even in the case of relatively thick gold layers. Combination of our nanopillar arrays with a transparent support material (glass) endows them with a unique feature compared to the commercially available (Si-based) substrates with no possibility for detection from the support side (Figure 4A). The light gray bars of Figure 4B represent the signal of the same samples analyzed earlier from the air side but, in this setup, with light arriving to the analyte spot through the glass support and the perforated gold layer. The collected signal changes only slightly with the gold thickness and is very similar to the signal collected from the air side up to 130 nm. Above 150 nm gold thickness, the "support side" signal intensity is less than 25% of the one detected from the air side (Figure 4A), and a significant absolute decrease is observed in the case of the 200 nm samples. At this gold thickness, the lift-off process (bead removal) becomes more difficult, resulting also in less reproducible enhancement results (not shown). Thus, the effectiveness of the measurements from the support side requires the combination of extraordinary transmission and successful lift-off. The transparent nature

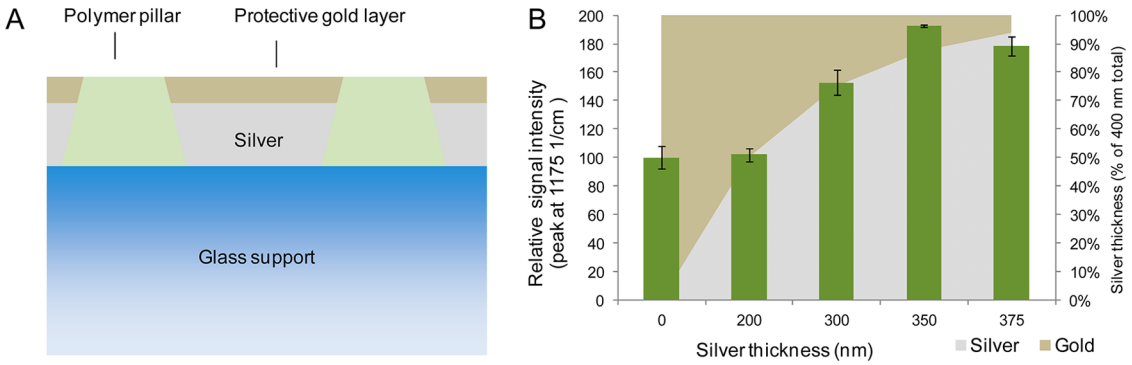

Figure 5. (A) Schematic structure of the chips with silver and protective gold metal layers. (B) Relative SERS signal intensity of malachite green (dried spots) on the surface of multi-metal (silver + gold) layer chips with a total metal thickness of 400 nm, protective gold layer on top (25−400 nm), and 633 nm excitation wavelength.

of the substrate allows detection from the support side, enabling combination of these surfaces even with reduced optical transparency microfluidic devices. Liquid samples (including cell suspensions) can be analyzed, or microarrays can be scanned by equipment with arbitrary optical orientation (Figure 4A).

Bimetallic Structures. Optical properties of silver nanohole arrays are described to be dependent on the geometrical parameters similarly to that of gold films.[29] Compared to gold, silver is known to be a metal with lower absorption in the visible range that causes a longer propagation length of the surface plasmon, allowing a stronger coupling of the resonance modes. From a practical point of view, silver is also cheaper but, at the same time, chemically less resistant than gold. As oxidation changes the physicochemical surface characteristics of the metal, silver nanomaterials (including thin films)—despite their excellent enhancer properties in SERS—without surface protection can hardly become competitors of gold-based products because of their inferior stability. Bimetallic Ag−Au nanohole arrays were reported to provide better enhancement than pure metals in SPR experiments, and the improved optical properties were correlated to the position of the plasmonic bands shifted depending on the metallic composition.[32]

Protecting the chemically sensitive metal surface with a more resistant metal layer might also solve the problem of stability.[33] For this reason, we tested the SERS enhancing properties of multilayer metal films (Figure 5A) in samples with 1000 nm pitch and a total film thickness of 400 at 633 nm excitation wavelength. Using 350 nm silver below 50 nm of gold as the protective layer (87.5% silver in the metal film), the signal intensity collected from dried spots of the Raman-active dye (malachite green) has been roughly doubled compared to that of pure gold samples (Figure 5B).

The enhancement increases with the silver proportion but decreases below 50 nm gold thickness again, most likely because of the combined effect of the grain size in the vapor-deposited gold layer affecting the plasmonic properties of the gold and the porosity of the protective layer that does not allow complete isolation of the silver from the oxidative atmosphere.

In addition to the improved plasmonic properties, gold can be easily modified using thiols. Thiolated oligonucleotides can be used for creating functionalized domains on the chip surface as well as for functionalization of the NPs and thiolated poly(ethylene glycol) for the passivation of the nonfunctionalized areas.

Repeatability and Scanning with DuoScan. Homogeneity of the signal collected from various locations on the surface has always been a challenging task for SERS substrates, as the enhancement strongly depends on the nanometrical features of the materials. We tested the repeatability of the signal obtained with our structure by measuring Raman spectra of a monolayer of malachite green isothiocyanate adsorbed on the gold surface which performed 36 different acquisitions distributed on an area of 50 × 50 μm of the substrate. Results (Figure 6, left) show a general good homogeneity of the surface with a standard deviation of about 13% calculated on the average signal of the peak at 1168 cm^{-1}.

In order to further increase the repeatability of the obtained data, we used the DuoScan acquisition mode developed by Horiba.[34] Applying this configuration, the laser spot, instead of being fixed on a single point, is continuously moved by a combination of scanning mirrors on an area having a defined shape and size. In this way, we were able to collect the signal from 36 different contiguous square regions (8 μm × 8 μm), thus covering the signal from the entire area of 50 × 50 μm^2 by spatial averaging the spectra. Thus, it has been possible to obtain a standard deviation of about 4% on the average signal (Figure 6, right) that is crucial for the reliable detection of the target molecules, but the average intensity appears to be lower because of the decreased laser density on the surface.

We relate the higher standard deviation that characterized the traditional acquisition mode to the fact that the pitch of the substrate is not negligible

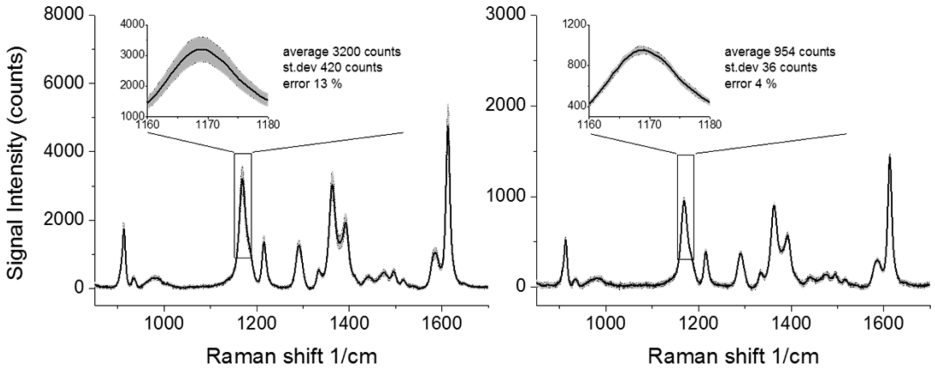

Figure 6. SERS spectra of a monolayer of malachite green isothiocyanate adsorbed on the SERS substrate acquired using the standard configuration of the microscope (left) and scanning the entire surface using the DuoScan acquisition mode (right). The solid line is the average of the 36 measurements used for the analysis, and the gray shadow represents the standard deviation. Insets in the two graphs show the peak at 1168 cm^{-1} used to calculate the error.

with respect to the dimension of the laser spot. As a consequence, a different number of polymeric pillars (and therefore of hot spots) can be illuminated by the laser depending on the position of the center of the laser beam relative to the period structure of the substrate. On the contrary, in DuoScan mode, the illuminated area is much larger and the number of analyzed pillars is quite constant, significantly improving the reproducibility of the results.

DNA Capture: Direct Labeled and Labeled Nanoparticle Strategy. Conventional DNA microarray techniques use fluorescently labeled oligonucleotide sequences for the detection of the captured target DNA. The undesired photobleaching of the organic fluorescent labels might be avoided by the application of quantum dots: NPs emitting fluorescent light. Still, this fluorescent signal can be quenched by other assay components. The fingerprint analysis of SERS labels offers an alternative to fluorescence almost independent from photobleaching with a high multiplexing capacity using a single excitation wavelength setup.

Direct labeling of oligonucleotides with Raman-active dyes often results in low stability products that are difficult to separate from the unreacted starting materials. Instead, in our system, oligonucleotides were coupled to SERS-active particles that were further functionalized with modified dye molecules: malachite green, rhodamine, and eosin isothiocyanate.[35] The strong binding of the isothiocyanate to gold results in a structure where the free surface between the already attached thiolated oligonucleotide chains becomes filled with high Raman cross section molecules (Figure 1). The particles can be easily separated from the unreacted organic compound and are stable in the annealing buffer. Besides the facile preparation method and stability, the labeled particles provide further signal enhancement due to a complex mechanism. The simplest component of this mechanism is the multiplication of the number of Raman scattering label molecules corresponding to one target oligonucleotide. Additionally, the Raman dyes are covalently bound to the surface of the SERS-active NPs, resulting in optimal configuration for the chemical component of the enhancement. They occupy ideal positions in very close proximity to the metal surface to interact with the localized surface plasmon, and after the particles are anchored to the chip surface, many of them appear in the hot spots generated between the NPs and the nanopillar array. The electromagnetic component of the enhancement becomes extremely high at positions close to the border of the holes, where (according to numerical calculations) the electromagnetic field distribution creates the highest SERS enhancement. Figure 1 illustrates the NPs captured on the gold surface, with an inset depicting a particle immobilized at the area with strongest electromagnetic field, creating a hot spot for the SERS detection of the labeling dye molecules. Figure 1B shows the scanning electron micrograph of the surface with the captured particles after the annealing reaction and rinsing with reaction buffer. According to the SEM image, most of the captured particles are located close to the polymeric pillars. This allows a 5-fold increase of the collected SERS signal in comparison to an analogous experiment performed on flat gold (Figure S3 in Supporting Information).

The relatively small (35−40 nm) DNA-funtionalized gold NPs exist as a stable suspension in the annealing buffer, and no significant sedimentation or deposition of the particles was observed under the conditions applied.

Microarray Results. The colloidal lithographic technique enables production of 2D plasmonic crystal surfaces over a few inches. The standard chips used in our experiments were about 1 cm × 2 cm, but even larger (3 cm × 6 cm) chips were fabricated with similar good homogeneity using the same manufacturing procedure (Figure S4 in Supporting Information). The dimensions of these substrates allow the deposition of microarrays on the chips and the identification of captured target molecules based on their position in the microarray. Figure 7 shows the results of a one-step

annealing experiment at various target (WT1 sequence) concentrations on a chip functionalized with a pattern of double columns of WT1-specific and ABL-specific (negative control) capture sequences. After we mapped the surface using the DuoScan mode of the Raman microscope and visualized the detected signal intensities as brightness of the scanned pixels, the images show the presence of the target gene (bright spots) and the absence of the negative control (dark areas at the positions of the ABL capture DNA).

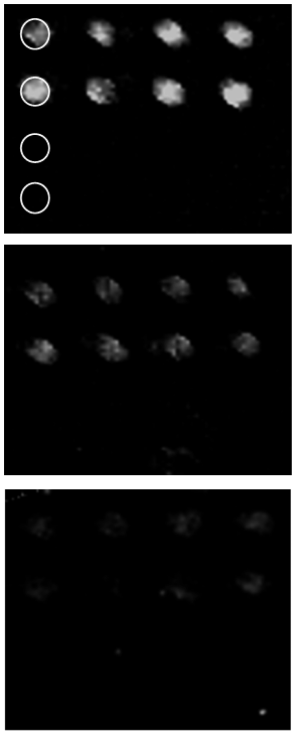

Figure 7. SERS-mapped image of the chip surface functionalized with WT1 capture oligonucleotide (first two lines in each frame) and ABL negative control capture oligonucleotide (third and fourth lines in each frame) at 200, 100, and 50 nM concentration of the target WT1 sequence (separate frames from top down). Circles in the first frame mark the position of the spots in the first row of the array. Brightness of the spots corresponds to signal peak (1170 cm^{-1}) intensity detected by the Raman microscope.

The brightness of the spots (corresponding to the SERS signal collected) is concentration-dependent, and the aspecific binding observed on spots functionalized with noncomplementary DNA is very low, practically equal to the binding on PEG-passivated areas. In a one-step assay system, where the target DNA has been put in contact with the functionalized surface (in the same moment) with the NPs, the detection limit (significantly higher detected signal than the signal collected from the passivated background) was found to be around 2 pM (Figure S5 in Supporting Information).

Multiplexing by SERS Fingerprint. Multiplexing on microarrays is provided by the known position of different functionalized domains (capture DNA spots) inside the array, but the real multiplexing capacity of SERS lies in the ability to distinguish chemical compounds based on their Raman fingerprint spectra. Figure 8A shows the spectral fingerprint of eosin, rhodamine, and malachite green isothiocyanate covalently bound to the surface of gold NPs. In a DNA array with domains covered by three different capture oligonucleotides (WT1, P-gp, and ABL), particles functionalized with the corresponding sequences become immobilized on the specific spots in the presence of the target DNA strands. Consequently, spots covered by NPs carrying the malachite green, eosin, or rhodamine label can be identified by registering the SERS intensity profile of corresponding spectra (LabSpec6, Horiba Jobin Yvon) after Raman mapping (Figure 8B).

This assay setup allows quantification of genetic markers using internal standards or complex mixtures containing reference (housekeeping) and target genes.

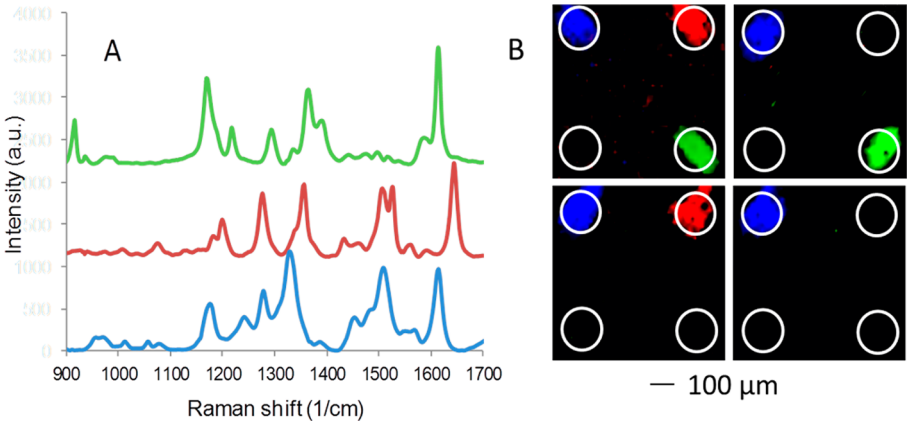

Figure 8. (A) SERS spectra of malachite green (green, top), rhodamine 6G (red, middle), and eosin (blue, bottom) isothiocyanate label on DNA-functionalized gold nanoparticles. (B) Raman maps of DNA microarray with different capture oligonucleotides: WT1, P-gp, polyA, and ABL, after annealing reaction with the target sequences and the oligonucleotide-functionalized Raman-labeled NPs. In the map at the top left, the target sequences of all the three genes (WT1, P-gp, ABL) were present in the incubation buffer. In the maps at the top right and bottom left, the target sequence of ABL and WT1 or P-gp was present, respectively. In the map at the bottom right, only the target sequence of ABL was present in the incubation buffer. Domains functionalized by different thiolated sequences can be clearly identified.

CONCLUSIONS

In contrast to the beam lithographical techniques that cannot provide enough covered surface area and acceptably high volume production for practical applications, cheap and well-reproducible nanopillar arrays manufactured by colloidal lithography and plasma deposition on a simple glass slide might become competitors of the actually available SERS solid substrates usually based on the use of silicon. Indeed, this plasmonic substrate can be obtained using techniques that are compatible with large production yields over large nanostructured areas (up to 6 in.) with state-of-the-art reproducibility. Moreover, properties of the 2D nanopillar array can be tailored to give optimal enhancement by tuning to fit the instrument and assay parameters. In this case, a 400 nm pitch and 200 nm "hole" diameter nanopillar array (with hexagonal symmetry) was chosen to match the excitation wavelength of a HeNe laser (633 nm), which is one of the cheapest laser sources and one of the most effective laser lines available for SERS experiments.[36] The favorable Raman enhancing behavior of this structure can be explained by the intensity and relative position of the substrate's localized plasmon resonance peak, the excitation wavelength, and the Raman-scattered light frequency.

Based on our results, excellent Raman enhancing properties accompanied by tunability, facile functionalization, and low production cost make nanopillar arrays promising for bioanalytical applications. The availability of cheap, reliable, and easy to use SERS substrates paves the road for development of bioanalytical tests that can be used in clinical practice. Among them, our nanopillar array and nanoparticle-based detection system combined with the concept of microspotted DNA arrays and Raman mapping are capable of providing quantitative information about expression levels of genes that are considered to be relevant markers in minimal residual disease monitoring. As proof-of-concept, we tested the capacity of a SERS-based bioassay for multiple detection of a leukemia marker using the WT1 sequence as the target and ABL sequence as the housekeeping reference gene. This heterogeneous reaction system built from a functionalized 2D gold nanopillar array and Raman-dye-modified gold NPs is able to detect simultaneously more gene sequences in a specific and sensitive way.

The resulting SERS sandwich assay is characterized by a detection limit of 2 pM that is very close to the one that can be reached using electrochemical-based approaches (in the femtomolar range).[37] It can benefit from the ability of detecting multiple target sequences typical of optical-based approaches and especially of SERS. These results are made possible by the particular high enhancement of the signal obtained through the hot spots given by the coupling of the localized surface plasmon present on the substrate[28] and the one on gold NPs. This additional enhancement of the Raman signal intensity allows improvement of the detection limit with respect to the standard SERS-based assay usually performed on top of a plain gold slide[38] or by the random aggregation of nanoparticles where the localization of the Raman dye inside the hot spot is less efficient.[39]

As the developed system is based on glass and signals that can be acquired through the support, it is possible that, as a future development, the integration of this system with microfluidic devices could be of great interest especially for the detection of multiple protein biomarkers directly in plasma.[40]

MATERIALS AND METHODS

Chemicals for the substrate preparation and reagents for the nanoparticle synthesis and functionalization were purchased from Sigma-Aldrich and used without further purification unless it is stated otherwise. Polystyrene beads and isothiocyanate-functionalized dye molecules were purchased from Life Technologies, and thiol-modified (5′) oligonucleotides were from Primm S.r.l. (Milano, Italy).

Manufacturing of the Gold-Embedded Nanopillar Arrays. The nanopillar arrays used in this study were prepared on a custom base by Plasmore S.r.l. according to the method described previously for the preparation of a similar nanostructure used for SPR applications.[28] Briefly, a monolayer of polystyrene beads arranged in a 2D hexagonal lattice was deposited on a glass slide coated with poly(acrylic acid) (ppAA). The samples were etched by plasma oxygen to reduce the beads' dimension and to remove uncovered ppAA. Afterward, a gold layer was deposited, and the beads were removed using an ultrasonic bath.

Morphological Evaluation. In order to evaluate morphological characteristics of the nanopillar arrays, SEM images of the surface (from the air side) were taken using a Hitachi TM-3000 SEM, at 15 kV acceleration voltage. The polymeric pillars appeared as darker areas, embedded in a brighter background of the gold film. Moreover, images of substrates which were not exposed to the lift-off process showed the presence of nanospheres, and in the same way, it was possible to control and verify the complete removal of PS particles on the surface. SEM images of the substrate after the annealing with the target sequences and gold nanoparticles were generated by a FEI-Nova Nanolab 600I microscope operating at 30 kV, available at the Nanobiosciences Unit, IHCP, Joint Research Centre, Ispra, Italy.

Optical Characterization. Reflectance measurements were applied for optical characterization of the chip surfaces. The measurements were performed with an inverted microscope (Axiovert 25, Zeiss) coupled with a compact USB fiber optic spectrometer (USB4000, OceanOptics). A halogen lamp was used as the light source, and the spectra were acquired over the range from 400 to 1000 nm. Light was directed to the surface (from the glass substrate side) through a 5× objective with a NA = 0.13 (Epiplan 5x, Zeiss), and the back-reflected light was collected by the same objective lens.

Chemistry. The surface of the substrates was functionalized with the 5′-thiolated single-stranded DNA (ssDNA) oligonucleotides (Primm) complementary to the target sequence (in the case of WT1, corresponding to the reverse primer in a PCR-based, validated WT1 detection method[41−43]). Table 1 summarizes the sequences used as targets and for the functionalization of the surface and nanoparticles.

TABLE 1. Target and Capture Sequences Applied in the Experiments

gene	target	capture on chip	capture on NPs
WT1	CGCTATTCGCAATCAGGGTTACAGCACGGTCACCTTCGACGGGACGCCCAGCTACGGTCACACGCCC	GGGCGTGTGACCGTAGCT	TAACCCTGATTGCGAATAGCG
ABL	AACCTTTTCGTTGCACTGTATGATTTTGTGGCCAGTGGAGATAACACTCTAAGCATAACTAAAGGTGAAAAGCTCCGGGT	ACCCGGAGCTTTTCACCTTT	AATCATACAGTGCAACGAAAAGGTT
P-gp	TGCAGCATTGCTGAGAACATTGCCTATGGAGACAACAGCCGGGTGGTGTCACAGGAAGAGATTGTGAGGGCA	TGCCCTCACAATCTCTTCCTG	AATGTTCTCAGCAATGCTGCA
polyA		AAAAAAAAAAAAAAAAA	

The functionalization took place due to the thiol group on the DNA sequence that allowed the formation of a sulfhydryl-mediated binding between the oligonucleotide and the gold layer on the chip. The drops of 100 μM thiolated oligonucleotide solutions were deposited on the surface. After 30 min incubation at room temperature, the whole chip was washed with water in order to remove unbound DNA and then incubated in an ethanolic solution of 5 mM polyethylene glycol methylether thiol (PEG-SH). The chip was incubated for 1 h; in this way, the PEG-SH passivated the remaining parts of the chip that were not functionalized with oligonucleotide sequences, thus reducing the probability of aspecific DNA binding on the surface. The chip was rinsed with ethanol and then again with water in order to remove the unbound PEG molecules.

For micropatterning of the chip surface, the thiolated oligonucleotides were diluted in an acetate printing buffer (100 mM, pH 6.1) containing 5% glycerol and spotted using an S3 sciFLEXARRAYER (Scienion, Germany). The obtained three drop spots were about 150 μm in diameter with 500 μm pitch, allowing the deposition of 400 well-separated functionalized domains on a 1 cm $\times$ 1 cm area.

Gold Nanoparticle Synthesis and Functionalization. Spherical gold NPs with a diameter of about 40 nm (Supporting Information Figure S1) were synthesized using citrate as reducing agent according to the method of Frens.[44] The resulting NP suspension was diluted 1:1 in sterile water. An aliquote of 20 μL of 100 μM thiolated oligonucleotide solution was added to 1 mL of NPs in a glass vial. The NPs were functionalized with the 5′-thiolated ssDNA oligonucleotide (Primm) by applying citrate buffer to trigger the DNA attachment to the particles.[45] After 5 min of incubation with thiolated oligonucleotides at room temperature, 100 μL of 200 mM sodium citrate buffer (pH 3) was mixed with the suspension by gentle shaking. The resulting mixture was incubated for 1 h in the dark followed by the addition of 10 μL of 100 μM rhodamine isothiocyanate or malachite green isothiocyanate solution and additional incubation in the dark for 30 min. In the case of eosin isothiocyanate, dye molecules were added first to particles followed by the already described addition of DNA and citrate buffer. After the incubation period, the particles were centrifuged and washed with a Tris-acetate buffer (25 mM, 100 mM NaCl, pH 8.5) in order to remove the unbound DNA and dye molecules. Then the washing buffer was changed to the saline sodium citrate (2xSSC) annealing buffer (300 mM NaCl, 30 mM sodium citrate, 0.01% SDS, pH 7) by a second separation and resuspension step.

In order to assess the correct functionalization of NPs with the oligonucleotide, 100 + 100 μL suspensions of NPs conjugated with the adjacent capture sequences of the WT1 gene were prepared and mixed with 2 μL of 10 μM WT1 sequence to induce the aggregation of the nanoparticles. The annealing reaction was confirmed by the color change of the solution from red to bluish, as described by Mirkin and co-workers[46] (Figure S2 in Supporting Information).

DNA Annealing. The substrate, functionalized with thiolated oligonucleotides and covered with PEG-SH, was dipped in a 200 μL suspension of functionalized gold nanoparticles followed by addition of the target DNA. Concentrations of target DNA tested in these experiments were in the range of 2 pM to 200 nM.

The sequence of the WT1 DNA target (67 base long ssDNA oligonucleotide, Table 1), which includes a part of exon 1 and exon 2 of the WT1 gene, was complementary to both of the two thiolated sequences that were used for functionalization of the substrate and the particles. The ABL and Pg-p model targets were 79 and 72 base long sequences from the ABL and P-gp gene coding strands, respectively (Table 1). The target DNA sequences were able to specifically immobilize a gold nanoparticle conjugated with Raman reporter molecules on the plasmonic array because both nanoparticles and the surface were conjugated with DNA probes that bind to different portions of the target sequence. The annealing reaction between the complementary sequences was performed by heating the sample to 70 °C for 4 min and cooling it slowly to 37 °C. The reaction was performed in a saline sodium citrate (2xSSC) annealing buffer (300 mM NaCl, 30 mM sodium citrate, 0.01% SDS, pH 7).

Finally, the chip was washed with the same 2xSSC buffer at 37 °C two times. After being dried, the active surface was scanned with the Raman microscope in order to collect the strongly enhanced Raman signal originating mainly from the reporter molecules laying in the so-called "hot spots" situated between the particles and the chip surface after the annealing reaction.

In order to be able to estimate the nonspecific binding in the sample, a negative control was prepared every time, where the target sequence was not added. The comparison between Raman signals obtained from the sample and from the negative control served to evaluate the specificity and the sensitivity of this system.

SERS Measurements. Raman spectra were acquired using an Aramis Horiba Jobin Yvon Raman microscope equipped with three laser lines with different wavelengths of 532, 633, and 785 nm. The sample was positioned under the Raman microscope usually in the "air side" up position to acquire a signal at different points or areas of the chip and to evaluate specificity and sensitivity for the detection of the DNA target. Samples were placed in the "support side" up position in the microscope when analyzing the effect of substrate orientation (Figure 4).

With this Raman instrument, it was possible to obtain a single spectrum from a specific point of the chip (about 1.5 μm diameter) or to collect all spectra acquired from a selected area on the surface (mapping). Analyzing spectral maps using the LabSpec 6 software of Horiba allowed visualization of the microspotted DNA arrays after annealing reaction with the Raman-labeled NPs. The DuoScan function of the Raman microscope was used to acquire spectra in mapping mode. The DuoScan acquisition is a technology based on a combination of scanning mirrors that move the laser beam across the surface, allowing light collection from a larger area, in our case 50 μm $\times$ 50 μm. Earlier, we found that this acquisition mode successfully decreases the signal intensity deviations caused by surface inhomogeneity in the case of some solid substrates.[25]

Raman images were baseline-corrected, and different spectra were automatically recognized through a classical least square analysis that was demonstrated to be able to distinguish the spots corresponding to the different sequences without the necessity of identifying a peak univocally related to the selected dye or previously knowing the position of the spot on the surface. Once the spots were identified, the intensity of the peaks was used for the concentration dependence experiments.

Conflict of Interest: The authors declare the following competing financial interest(s): As shareholders of Plasmore S.r.l., Gerardo Marchesini and Andrea Valsesia declare a financial interest in this work.

Acknowledgment. Funding for this research was provided by Fondazione Cariplo (International Recruitment Call 2011 Project: An innovative, nanostructured biosensor for early diagnosis and minimal residual disease assessment of cancer, using

surface-enhanced Raman spectroscopy), by the Italian Ministry of Health (Conto Capitale 2010: Realizzazione e validazione di una core facility di biofotonica clinica per diagnosi precocee monitoraggio di minimal residual disease in patologie tumorali) and under the frame of EuroNanoMed II (European Innovative Research & Technological Development PRrojects in Nanomedicine) InNaSERSS: Development of Integrated Nanorray based SERS System for Leukemia biomarker detection.

Supporting Information Available: Characterization of Au nanoparticles; annealing between DNA-functionalized Au nanoparticles; comparison of the sandwich assay on the substrate *vs* flat gold; homogeneity of SERS enhancement on a large area; and detection limit of the SERS assay. This material is available free of charge *via* the Internet at http://pubs.acs.org.

REFERENCES AND NOTES

1. Graham, D. The Next Generation of Advanced Spectroscopy: Surface Enhanced Raman Scattering from Metal Nanoparticles. *Angew. Chem., Int. Ed.* **2010**, *49*, 9325–9327.
2. Kirschner, C.; Maquelin, K.; Pina, P.; Ngo Thi, N. A.; Choo-Smith, L. P.; Sockalingum, G. D.; Sandt, C.; Ami, D.; Orsini, F.; Doglia, S. M.; *et al.* Classification and Identification of Enterococci: A Comparative Phenotypic, Genotypic, and Vibrational Spectroscopic Study. *J. Clin. Microbiol.* **2001**, *39*, 1763–1770.
3. Nguyen, C. T.; Nguyen, J. T.; Rutledge, S.; Zhang, J.; Wang, C.; Walker, G. C. Detection of Chronic Lymphocytic Leukemia Cell Surface Markers Using Surface Enhanced Raman Scattering Gold Nanoparticles. *Cancer Lett.* **2010**, *292*, 91–97.
4. Liu, G. L.; Chen, F. F.; Ellman, J. A.; Lee, L. P. Peptide–Nanoparticle Hybrid SERS Probe for Dynamic Detection of Active Cancer Biomarker Enzymes. *Conf. Proc. IEEE Eng. Med. Biol. Soc.* **2006**, *1*, 795–798.
5. Hering, K.; Cialla, D.; Ackermann, K.; Dorfer, T.; Moller, R.; Schneidewind, H.; Mattheis, R.; Fritzsche, W.; Rosch, P.; Popp, J. SERS: A Versatile Tool in Chemical and Biochemical Diagnostics. *Anal. Bioanal. Chem.* **2008**, *390*, 113–124.
6. Deschler, B.; Lubbert, M. Acute Myeloid Leukemia: Epidemiology and Etiology. *Cancer* **2006**, *107*, 2099–2107.
7. American Cancer Society. *Cancer Facts and Figures 2013*; American Cancer Society: Atlanta, GA, **2013**.
8. Sant, M.; Allemani, C.; Tereanu, C.; De Angelis, R.; Capocaccia, R.; Visser, O.; Marcos-Gragera, R.; Maynadie, M.; Simonetti, A.; Lutz, J. M.; *et al.* Incidence of Hematologic Malignancies in Europe by Morphologic Subtype: Results of the HAEMACARE Project. *Blood* **2010**, *116*, 3724–3734.
9. Schuurhuis, G. J.; Broxterman, H. J.; Ossenkoppele, G. J.; Baak, J. P.; Eekman, C. A.; Kuiper, C. M.; Feller, N.; van Heijningen, T. H.; Klumper, E.; Pieters, R.; *et al.* Functional Multidrug Resistance Phenotype Associated with Combined Overexpression of Pgp/MDR1 and MRP Together with 1-β-D-Arabinofuranosylcytosine Sensitivity May Predict Clinical Response in Acute Myeloid Leukemia. *Clin. Cancer Res.* **1995**, *1*, 81–93.
10. Glavinas, H.; Krajcsi, P.; Cserepes, J.; Sarkadi, B. The Role of ABC Transporters in Drug Resistance, Metabolism and Toxicity. *Curr. Drug Delivery* **2004**, *1*, 27–42.
11. Sharom, F. J. The P-Glycoprotein Multidrug Transporter. *Essays Biochem.* **2011**, *50*, 161–178.
12. Paietta, E. Minimal Residual Disease in Acute Myeloid Leukemia: Coming of Age. *Hematology* **2012**, *2012*, 35–42.
13. Estey, E.; Dohner, H. Acute Myeloid Leukemia. *Lancet* **2006**, *368*, 1894–1907.
14. Shaffer, B. C.; Gillet, J. P.; Patel, C.; Baer, M. R.; Bates, S. E.; Gottesman, M. M. Drug Resistance: Still a Daunting Challenge to the Successful Treatment of AML. *Drug Resist. Updates* **2012**, *15*, 62–69.
15. Wittwer, C. T.; Herrmann, M. G.; Gundry, C. N.; Elenitoba-Johnson, K. S. Real-Time Multiplex PCR Assays. *Methods* **2001**, *25*, 430–442.
16. Jorgensen, J. L.; Chen, S. S. Monitoring of Minimal Residual Disease in Acute Myeloid Leukemia: Methods and Best Applications. *Clin. Lymphoma, Myeloma Leuk.* **2011**, *11*, S49–53.
17. Steinbach, D.; Debatin, K. M. What Do We Mean by Sensitivity When We Talk About Detecting Minimal Residual Disease? *Leukemia* **2008**, *22*, 1638–1639.
18. Ross, D. M.; Branford, S.; Melo, J. V.; Hughes, T. P. Reply to 'What Do We Mean by Sensitivity When We Talk About Detecting Minimal Residual Disease?'. *Leukemia* **2009**, *23*, 819–820.
19. Rossi, G.; Minervini, M. M.; Carella, A. M.; de Waure, C.; di Nardo, F.; Melillo, L.; D'Arena, G.; Zini, G.; Cascavilla, N. Comparison between Multiparameter Flow Cytometry and WT1-RNA Quantification in Monitoring Minimal Residual Disease in Acute Myeloid Leukemia without Specific Molecular Targets. *Leuk. Res.* **2012**, *36*, 401–406.
20. Bergmann, L.; Miething, C.; Maurer, U.; Brieger, J.; Karakas, T.; Weidmann, E.; Hoelzer, D. High Levels of Wilms' Tumor Gene (wt1) mRNA in Acute Myeloid Leukemias Are Associated with a Worse Long-Term Outcome. *Blood* **1997**, *90*, 1217–1225.
21. Willasch, A. M.; Gruhn, B.; Coliva, T.; Kalinova, M.; Schneider, G.; Kreyenberg, H.; Steinbach, D.; Weber, G.; Hollink, I. H.; Zwaan, C. M.; *et al.* Standardization of WT1 mRNA Quantitation for Minimal Residual Disease Monitoring in Childhood AML and Implications of WT1 Gene Mutations: A European Multicenter Study. *Leukemia* **2009**, *23*, 1472–1479.
22. Kleinman, S. L.; Frontiera, R. R.; Henry, A.-I.; Dieringer, J. A.; Van Duyne, R. P. Creating, Characterizing and Controlling Chemistry with SERS Hot Spots. *Phys. Chem. Chem. Phys.* **2013**, *15*, 21–36.
23. Dougan, J. A.; Faulds, K. Surface Enhanced Raman Scattering for Multiplexed Detection. *Analyst* **2012**, *137*, 545–554.
24. Liu, B.; Zhou, P.; Liu, X.; Sun, X.; Li, H.; Lin, M. Detection of Pesticides in Fruits by Surface-Enhanced Raman Spectroscopy Coupled with Gold Nanostructures. *Food Bioprocess Technol.* **2013**, *6*, 710–718.
25. Mehn, D.; Morasso, C.; Vanna, R.; Bedoni, M.; Prosperi, D.; Gramatica, F. Immobilised Gold Nanostars in a Paper-Based Test System for Surface-Enhanced Raman Spectroscopy. *Vibr. Spectrosc.* **2013**, *68*, 45–50.
26. Perney, N. M. B.; Baumberg, J. J.; Zoorob, M. E.; Charlton, M. D. B.; Mahnkopf, S.; Netti, C. M. Tuning Localized Plasmons in Nanostructured Substrates for Surface-Enhanced Raman Scattering. *Opt. Express* **2006**, *14*, 847–857.
27. Schmidt, M. S.; Hübner, J.; Boisen, A. Large Area Fabrication of Leaning Silicon Nanopillars for Surface Enhanced Raman Spectroscopy. *Adv. Mater.* **2012**, *24*, OP11–OP18.
28. Giudicatti, S.; Valsesia, A.; Marabelli, F.; Colpo, P.; Rossi, F. Plasmonic Resonances in Nanostructured Gold/Polymer Surfaces by Colloidal Lithography. *Phys. Status Solidi A* **2010**, *207*, 935–942.
29. Ahmadreza, H.; Mojtaba, K.; Vo-Van, T. Optical Behaviour of Thick Gold and Silver Films with Periodic Circular Nanohole Arrays. *J. Phys. D: Appl. Phys.* **2012**, *45*, 485105.
30. Bottazzi, B.; Fornasari, L.; Frangolho, A.; Giudicatti, S.; Mantovani, A.; Marabelli, F.; Marchesini, G.; Pellacani, P.; Therisod, R.; Valsesia, A. Multiplexed Label-Free Optical Biosensor for Medical Diagnostics. *J. Biomed. Opt.* **2014**, *19*, 017006.
31. Sharma, B.; Fernanda Cardinal, M.; Kleinman, S. L.; Greeneltch, N. G.; Frontiera, R. R.; Blaber, M. G.; Schatz, G. C.; Van Duyne, R. P. High-Performance SERS Substrates: Advances and Challenges. *MRS Bull.* **2013**, *38*, 615–624.
32. Murray-Méthot, M.-P.; Ratel, M.; Masson, J.-F. Optical Properties of Au, Ag, and Bimetallic Au on Ag Nanohole Arrays. *J. Phys. Chem. C* **2010**, *114*, 8268–8275.
33. Zynio, S.; Samoylov, A.; Surovtseva, E.; Mirsky, V.; Shirshov, Y. Bimetallic Layers Increase Sensitivity of Affinity Sensors Based on Surface Plasmon Resonance. *Sensors* **2002**, *2*, 62–70.
34. Horiba Jobin Yvon. *DuoScan Imaging*, **2012**.
35. Li, M.; Cushing, S. K.; Liang, H.; Suri, S.; Ma, D.; Wu, N. Plasmonic Nanorice Antenna on Triangle Nanoarray for Surface-Enhanced Raman Scattering Detection of Hepatitis B Virus DNA. *Anal. Chem.* **2013**, *85*, 2072–2078.
36. Morasso, C.; Mehn, D.; Vanna, R.; Bedoni, M.; Forvi, E.; Colombo, M.; Prosperi, D.; Gramatica, F. One-Step

Synthesis of Star-like Gold Nanoparticles for Surface Enhanced Raman Spectroscopy. *Mater. Chem. Phys.* **2014**, *143*, 1215–1221.
37. Drummond, T. G.; Hill, M. G.; Barton, J. K. Electrochemical DNA Sensors. *Nat. Biotechnol.* **2003**, *21*, 1192–1199.
38. Braun, G.; Lee, S. J.; Dante, M.; Nguyen, T. Q.; Moskovits, M.; Reich, N. Surface-Enhanced Raman Spectroscopy for DNA Detection by Nanoparticle Assembly Onto Smooth Metal Films. *J. Am. Chem. Soc.* **2007**, *129*, 6378–6379.
39. Feuillie, C.; Merheb, M. M.; Gillet, B.; Montagnac, G.; Daniel, I.; Hanni, C. A Novel SERRS Sandwich-Hybridization Assay To Detect Specific DNA Target. *PLoS One* **2011**, *6*, e17847.
40. Li, M.; Cushing, S. K.; Zhang, J.; Suri, S.; Evans, R.; Petros, W. P.; Gibson, L. F.; Ma, D.; Liu, Y.; Wu, N. Three-Dimensional Hierarchical Plasmonic Nano-Architecture Enhanced Surface-Enhaced Raman Scattering Immunosensor for Cancer Biomarker Detection in Blood Plasma. *ACS Nano* **2013**, *7*, 4967–4976.
41. Van Dijk, J. P.; Knops, G. H.; Van De Locht, L. T.; Menke, A. L.; Jansen, J. H.; Mensink, E. J.; Raymakers, R. A.; De Witte, T. Abnormal WT1 Expression in the CD34-Negative Compartment in Myelodysplastic Bone Marrow. *Br. J. Hamaetol.* **2002**, *118*, 1027–1033.
42. Gabert, J.; Beillard, E.; van der Velden, V. H.; Bi, W.; Grimwade, D.; Pallisgaard, N.; Barbany, G.; Cazzaniga, G.; Cayuela, J. M.; Cave, H.; *et al.* Standardization and Quality Control Studies of 'Real-Time' Quantitative Reverse Transcriptase Polymerase Chain Reaction of Fusion Gene Transcripts for Residual Disease Detection in Leukemia: A Europe Against Cancer Program. *Leukemia* **2003**, *17*, 2318–2357.
43. Beillard, E.; Pallisgaard, N.; van der Velden, V. H.; Bi, W.; Dee, R.; van der Schoot, E.; Delabesse, E.; Macintyre, E.; Gottardi, E.; Saglio, G.; *et al.* Evaluation of Candidate Control Genes for Diagnosis and Residual Disease Detection in Leukemic Patients Using 'Real-Time' Quantitative Reverse-Transcriptase Polymerase Chain Reaction (RQ-PCR): A Europe Against Cancer Program. *Leukemia* **2003**, *17*, 2474–2486.
44. Frens, G. Controlled Nucleation for the Regulation of the Particle Size in Monodisperse Gold Suspensions. *Nature* **1973**, *241*, 20–22.
45. Zhang, X.; Servos, M. R.; Liu, J. Instantaneous and Quantitative Functionalization of Gold Nanoparticles with Thiolated DNA Using a pH-Assisted and Surfactant-Free Route. *J. Am. Chem. Soc.* **2012**, *134*, 7266–7269.
46. Mirkin, C. A.; Letsinger, R. L.; Mucic, R. C.; Storhoff, J. J. A DNA-Based Method for Rationally Assembling Nanoparticles into Macroscopic Materials. *Nature* **1996**, *382*, 607–609.